Icarus 226 (2013) 1241–1251

Contents lists available at ScienceDirect

Icarus

journal homepage: www.elsevier.com/locate/icarus

Integrating radar stratigraphy with high resolution visible stratigraphy of the north polar layered deposits, Mars

S. Christian [a,*], J.W. Holt [a], S. Byrne [b], K.E. Fishbaugh [c]

[a] The Jackson School of Geosciences, University of Texas, Austin, TX 78712, USA
[b] Lunar and Planetary Laboratory, University of Arizona, Tucson, AZ 85745, USA
[c] Center for Earth and Planetary Studies, Smithsonian National Air and Space Museum, Washington, DC 20013, USA

ARTICLE INFO

Article history:
Received 28 January 2013
Revised 16 June 2013
Accepted 3 July 2013
Available online 13 July 2013

Keywords:
Mars
Mars, Polar geology
Mars, Polar caps
Radar observations

ABSTRACT

Shallow Radar (SHARAD) on board NASA's Mars Reconnaissance Orbiter has successfully detected tens of reflectors in the subsurface of the north polar layered deposits (NPLD) of Mars. Radar reflections are hypothesized to originate from the same material interfaces that result in visible layering. As a first step towards verifying this assumption, this study uses signal analyses and geometric comparisons to quantitatively examine the relationship between reflectors and visible layers exposed in an NPLD outcrop. To understand subsurface structures and reflector geometry, reflector surfaces have been gridded in three dimensions, taking into account the influence of surface slopes to obtain accurate subsurface geometries. These geometries reveal reflector dips that are consistent with optical layer slopes. Distance–elevation profiling of subsurface reflectors and visible layer boundaries reveals that reflectors and layers demonstrate similar topography, verifying that reflectors represent paleosurfaces of the deposit. Statistical and frequency-domain analyses of the separation distances between successive layers and successive reflectors confirms the agreement of radar reflector spacing with characteristic spacing of certain visible layers. Direct elevation comparisons between individual reflectors and discrete optical layers, while necessary for a one-to-one correlation, are complicated by variations in subsurface structure that exist between the outcrop and the SHARAD observations, as inferred from subsurface mapping. Although these complications have prevented a unique correlation, a genetic link between radar reflectors and visible layers has been confirmed, validating the assumption that radar reflectors can be used as geometric proxies for visible stratigraphy. Furthermore, the techniques for conducting a stratigraphic integration have been generalized and improved so that the integration can be undertaken at additional locations.

1. Introduction

Investigation of the astronomical theory of climate change prompted a revolution in the detection (Emiliani, 1955), correlation (Hays et al., 1969; Shackleton and Opdyke, 1973) and analysis (Hays et al., 1976; Imbrie and Imbrie, 1980) of periodic signals in Earth's geologic record. Testing the hypothesis of orbital climate forcing required an enormous effort in pioneering new techniques for the quantification of geological data. New paleoclimate proxies had to be discovered (Emiliani, 1955), and accepted methods and interpretations had to be reevaluated and altered (Shackleton, 1967) or even abandoned entirely (Kukla, 1977). The hypothesis was ultimately confirmed by synthesizing multiple records, including sedimentary, geochemical and paleomagnetic, that when integrated provided a comprehensive history of Earth's climate cycles (Imbrie, 1982).

Concurrent with rapid advances occurring in terrestrial climate science, the discovery of layering in the polar deposits of Mars (Murray et al., 1972; Figs. 1b and 2) provided the only empirical evidence for periodic climate change on a planet other than Earth (Cutts et al., 1976) and excited the prospect of a robust martian climate record (Cutts, 1973). The expectation of discovering such a record in the stratigraphy of the polar layered deposits (PLD) has persisted (Fishbaugh et al., 2008), leading to a sustained effort to fully characterize layering (Fishbaugh et al., 2010a). As a result, determining the optical (Blasius et al., 1982; Fishbaugh and Hvidberg, 2006), spectral (Milkovich and Head, 2005; Perron and Huybers, 2009), and radar (Picardi et al., 2005; Phillips et al., 2008) characteristics of the PLD remains an active area of research (Fishbaugh et al., 2008).

Two leading perspectives of PLD stratigraphy have emerged from the resultant studies. High resolution images from Mars Reconnaissance Orbiter's (MRO) High Resolution Imaging Science Experiment (HiRISE) (McEwen et al., 2007) and Context Camera (CTX) (Malin et al., 2007) have prompted spatially-isolated,

* Corresponding author.
E-mail address: schristian@utexas.edu (S. Christian).

0019-1035/$ - see front matter © 2013 Elsevier Inc. All rights reserved.
http://dx.doi.org/10.1016/j.icarus.2013.07.003

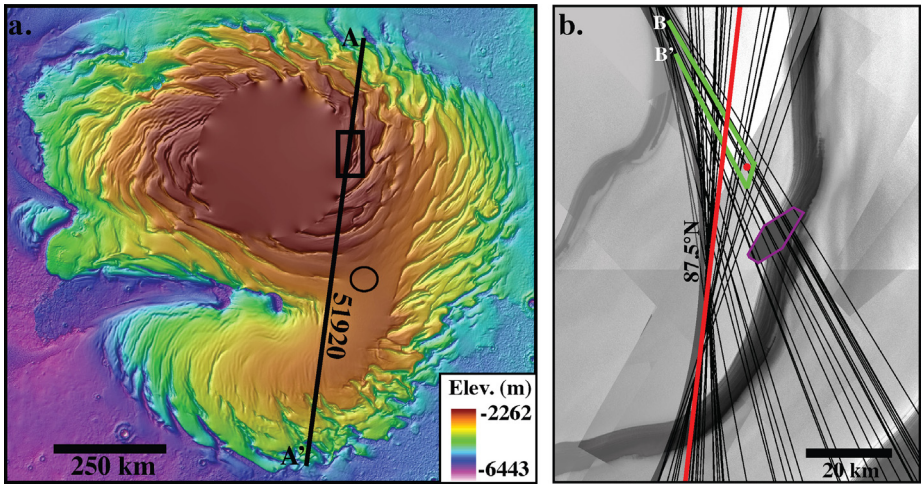

Fig. 1. (a) Mars Orbiter Laser Altimeter (MOLA) topography of Planum Boreum overlain by a hillshade. Context box shows location of Fig. 1b. SHARAD observation 51920 is shown in Fig. 3. Circle denotes area containing line intersections used in the crossover analysis. (b) Study site of data set integration. Black lines show SHARAD observations used to construct subsurface interfaces. Observation 51920 is shown in red, and transect B–B′ (shown in green) gives the location of Fig. 4. The location of a model radar trace is denoted by a red circle. The DEM footprint is shown in gray, outlined in purple.

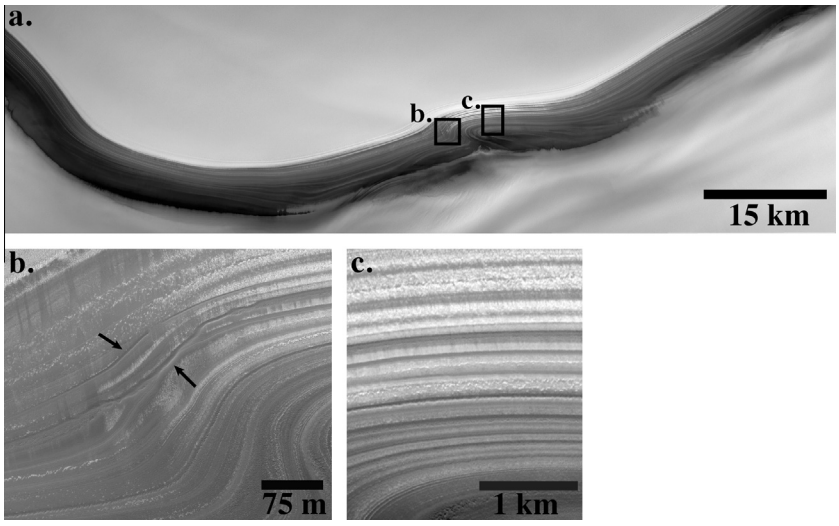

Fig. 2. (a) CTX image P02_001738_2671 shows layering at the study site at a resolution of 6 m/pixel. (b and c) are subimages of HiRISE image PSP_001871_2670 and show layers in high resolution (25 cm/pixel). An angular truncation surfaces, denoted by arrows, are visible in (b).

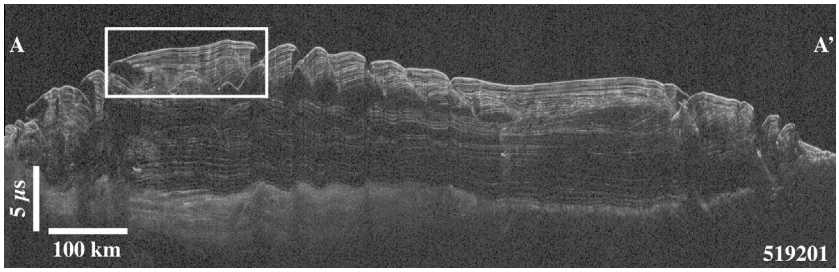

Fig. 3. SHARAD observation 519201. The location of the subsurface study site is outlined by the white box. Transect location is shown in Fig. 1a.

morphologically- and topographically-detailed descriptions of the north PLD (NPLD) surface (Fishbaugh et al., 2010a, 2010b). In contrast to the meter-scale description and delineation of surficial expressions of layering, MRO's Shallow Radar (SHARAD) (Seu et al., 2007) has resolved material changes in the NPLD subsurface (Phillips et al., 2008; Fig. 3). As a result, the definition of an internal radar stratigraphy over 100s of kilometers is possible (Putzig et al., 2009; Holt et al., 2010), albeit at an order of magnitude lower resolution than is common in surface studies (McEwen et al., 2007; Seu et al., 2007).

Apparent repetitions in both visible (Laskar et al., 2002; Milkovich and Head, 2005; Fig. 2) and radar (Phillips et al., 2008;

Fig. 3) stratigraphies have been proposed to correlate to martian insolation cycles. The results, however, have been neither unique (Putzig et al., 2009) nor robust (Fishbaugh et al., 2010a). Failure to address the question of martian climate cycles and the influence of orbital forcing using individual polar data sets is reminiscent of the difficulties experienced in the terrestrial case decades before (Imbrie, 1982). This suggests that a similar approach, namely the integration and correlation of multiple signals, must be attempted in order to reconstruct a complete climate record for the NPLD.

Both radar and optical stratigraphies are the hypothesized result of the changing ratio of siliciclastic impurities to water ice in the NPLD (Nunes and Phillips, 2006; Grima et al., 2009). Through a shared origin, these signals provide the opportunity to attempt a stratigraphic integration and correlation, which first requires an understanding of the relationship between morphologically distinct visible layers and radar reflectors. While this relationship has been qualitatively explored in the south PLD (SPLD) (Milkovich et al., 2009), a diverse suite of high resolution tools (McEwen et al., 2007; Seu et al., 2007) and techniques (Fishbaugh et al., 2010a, 2010b; Putzig et al., 2009; Holt et al., 2008) applied to the NPLD has made a quantitative investigation possible. Analyzing morphologic and topographic properties of surface layering detected by HiRISE (Fishbaugh et al., 2010a, 2010b) in conjunction with subsurface structure and stratigraphy revealed by SHARAD (Putzig et al., 2009; Holt et al., 2010) will begin to define the relationship between visible layering and radar reflectors.

The union of stratigraphic information from optical and radar sources at divergent resolutions and spatial scales would ideally provide not only a comprehensive understanding of NPLD structure and stratigraphy in three dimensions, but also would supply the key to a climate record spanning multiple time scales (Milkovich and Head, 2005; Phillips et al., 2008). Such a union has been envisioned as the correlation of a single reflector to one or many discrete visible layers (Milkovich et al., 2009). It is, however, important to note that the hypothesis of a shared mechanism between the stratigraphies (Nunes and Phillips, 2006) has not yet been empirically tested. The objectives of this work, therefore, are to examine the assumption of a shared mechanism between visible layering and radar reflectance by comparison of the topographic, spectral and statistical properties of each; to evaluate the plausibility of a direct correlation between a single reflector and a visible layer or defined layer sequence; and to use the results there from to improve understanding of the relationship between radar and optical stratigraphies.

2. NPLD stratigraphy

2.1. Optical stratigraphy

Although based on low resolution imagery returned by the Mariner 9 and Viking Orbiter missions, early deductions of PLD composition, structure and stratigraphy have been supported by subsequent decades of research. Preliminary studies of the SPLD concluded that exposures exhibited "cliff-bench" topography resulting from static, near-horizontal, areally-extensive layers of ice and dust emplaced by air-fall deposition (Murray et al., 1972; Cutts, 1973). Topography returned by the Mars Orbiter Laser Altimeter (MOLA) and imagery from the Mars Orbiter Camera (MOC) have allowed for the verification of original structural inferences in modern study. At both poles layers consistently dip equatorward on the order of 1° (Byrne and Ivanov, 2004; Fishbaugh and Hvidberg, 2006) and demonstrate geometries inconsistent with flow (Byrne and Ivanov, 2004; Fishbaugh and Hvidberg, 2006). Furthermore, the topographic effects of erosionally-resistant bench forming layers in the south (Byrne and Ivanov, 2004) and marker beds in the north (Malin and Edgett, 2001; Fishbaugh et al., 2010a, 2010b) result in the stair-stepped topography proposed by early studies (Murray et al., 1972).

Large-scale continuity and uniformity of layering (Cutts, 1973) has recently been supported by the results of spectral wavelength matching (Milkovich and Head, 2005), as well as visual correlations of prominent layers (Byrne and Ivanov, 2004; Malin and Edgett, 2001) and layer sequences (Fishbaugh and Hvidberg, 2006) across hundreds of kilometers. The lateral extent of uniform layering has led to the wide acceptance of deposition by airfall sedimentation (Thomas et al., 1992), however, disruption by truncation surfaces indicating erosional episodes has also been recognized (Cutts et al., 1976). While erosional surfaces tend to be expressed locally and, in the NPLD, to proliferate around the deposit margins (Tanaka et al., 2005, 2008; Tanaka and Fortezzo, 2012), they also can occur at exposures in the interior (Fishbaugh et al., 2010b; e.g., Fig. 2c) and may represent periods of either local or regional erosion (Tanaka et al., 2008). Furthermore, large-scale change in the erosional morphology of NPLD layering (Herkenhoff et al., 2007) suggests a shift in depositional parameters and potentially indicates one or more disconformable surfaces. Disconformities in visible layering may relate to regional, buried unconformities apparent in the subsurface (Putzig et al., 2009; Holt et al., 2010), however this relationship has not yet been explicitly studied. The existence of such perturbations in otherwise uniform layering underscores the incompleteness of the stratigraphic record, while the uncertainty of their extent and interrelationships within the NPLD (Tanaka et al., 2008) highlights the limitations of image, or "outcrop," analysis.

With surficial data until recently the only means of studying PLD stratigraphy (Fishbaugh and Hvidberg, 2006), much consideration has been given to variables influencing the reliability of the surface expression of layers. Murray et al. (1972) first commented on the inconsistency of layer albedo, noting its frequent dependency on exposure orientation and curvature, but also identifying instances in which neither factor induced a change in brightness. While the discovery of dust and frost mantling deposits at the scale of hundreds of meters (Herkenhoff and Murray, 1990) suggested the inherent albedo of underlying layers might be largely masked, this could not be verified until imagery at sub-meter resolution demonstrated that apparent albedo is a function of layer topography, morphology and "younger mantling deposit" (YMD) (Fishbaugh et al., 2010a), thus making it an unreliable proxy for composition and a complicating factor in layer delineation (Herkenhoff et al., 2007; Fishbaugh et al., 2010a). Even though the consistency of layer correlations between troughs based on methods relying on apparent albedo (Milkovich and Head, 2005; Fishbaugh and Hvidberg, 2006; Milkovich et al., 2008) argues that some component of apparent albedo is inherent to the layers (Fishbaugh et al., 2010a), high resolution topographic and morphologic data may provide the most reliable means of delineating layer boundaries (Fishbaugh et al., 2010a, 2010b).

2.2. Radar stratigraphy

The arrival at Mars of orbital sounding radar has introduced additional complexity, but also opportunity, in the attempt to define a coherent stratigraphy for the NPLD. Mars Advanced Radar for Subsurface and Ionospheric Sounding (MARSIS) on board Mars Express (Picardi et al., 2005) demonstrated the ability of sounding radar to penetrate the icy subsurface to the base of Planum Boreum, but its theoretical resolution of 85 m in water ice (dielectric $\varepsilon = 3.1$) (Picardi et al., 2005; Seu et al., 2007) and unfavorable viewing geometry frequently did not permit the detection of internal reflectors in the NPLD (Picardi et al., 2005). Complementary to MARSIS' deep-sounding capabilities, the higher resolution

(theoretical vertical resolution of 8.5 m in water ice) provided by SHARAD (Seu et al., 2007) has allowed the distinction of tens of reflectors in the water–ice rich (Grima et al., 2009) NPLD subsurface (Phillips et al., 2008; Fig. 3), lending further credence to the name "layered deposits" and providing the opportunity to define a new type of NPLD stratigraphy.

As with optical imagery, in which delineating a layer has become a complicated task requiring knowledge of many surface characteristics (Fishbaugh et al., 2010), multiple methods for defining radar stratigraphy have been proposed. On one hand, prominent, alternating bands of reflector-rich and -poor zones have been identified as containing a potential climate record (Phillips et al., 2008), and the boundaries between pairs of these zones have been mapped in order to derive rough volume constraints (Putzig et al., 2009). On the other hand, the principles of sequence stratigraphy have been employed to identify significant periods of accumulation and erosion, resulting in a narrative of the history of Chamsa Boreale (Holt et al., 2010) and the prospect of similarly deciphering a history of accumulation for Planum Boreum. The large-scale focus of the radar studies, notably, forms the antithesis approach to that taken in the optical case and offers the opportunity to unify information at two scales in order to form a more complete understanding of Planum Boreum's past.

2.3. Integrated stratigraphy

Until recently, optical and radar stratigraphies have been largely interpreted in isolation, and when considered in unison, analysis has been primarily qualitative (Holt et al., 2010) or speculative (Herkenhoff et al., 2007). Ideally, a quantitative integration of high resolution outcrop stratigraphy with penetrative radar stratigraphy would allow for the maximum exploitation of each of these tools, resulting in a comprehensive stratigraphic framework for the NPLD. While optical studies at sub-meter resolution are spatially isolated and, by their surficial nature, lack significant information about subsurface structure, radar data are unable to distinguish the morphologic and topographic differences that may lend important geologic meaning to changes in composition. If evaluated in a unified context, however, specified radar sections within a large-scale structural context could be linked to morphologically-distinct layers in outcrop, which could then be traced over tens to hundreds of kilometers through the penetrative nature of the radar data, thus resolving the primary shortcomings of each dataset.

This ideal stratigraphic model, however, is predicated on the assumption of a shared mechanism between radar reflectance and visible layering. Early models of layer formation (Murray et al., 1972; Cutts, 1973; Cutts and Lewis, 1982) identified the likelihood of layers caused by varying fractions of dust or sand cemented by volatiles, with recent conclusions favoring a composition of predominantly pure water ice with small volumes of silicic impurities (Thomas et al., 1992). This conclusion has been supported by dielectric studies of the NPLD utilizing SHARAD, which suggest bulk purity of water ice in excess of 95% (Grima et al., 2009). Despite the high degree of purity, the distribution of impurities thought to result in visible layering also have been predicted to cause the dielectric changes that would give rise to radar reflectance (Nunes and Phillips, 2006), and one of the primary objectives of SHARAD was to use such changes to study the internal structure of the NPLD (Seu et al., 2007). The success of SHARAD in detecting multiple reflectors (Phillips et al., 2008), and the qualitative resemblance of those reflectors to visible layer geometries (Smith and Holt, 2010), has subsequently increased confidence in the concept that visible layers and reflectors are related. While no quantitative evidence has yet been presented to support this assumption, the following methods have been designed to test the relationship between layers and reflectors, and to begin to explore what type of "layer" a radar reflector might represent (Fishbaugh et al., 2010a).

3. Study site and datasets

All analyses presented in this work have been applied to a single NPLD exposure centered near 87.1°N, 93.0°E (Fig. 1). Optical data are from HiRISE and CTX, which provide ~25 cm/pixel (McEwen et al., 2007) and ~6 m/pixel (Malin et al., 2007) resolution, respectively. Morphological descriptions and boundary elevations of visible layers are from the stratigraphic analyses of Fishbaugh et al. (2010a) and Fishbaugh et al. (2010b), which used a digital elevation model (DEM) constructed from HiRISE stereopair PSP_001738_2670 and PSP_001871_2670 (Fig. 1b). Due to the small size of the DEM (~16 km in length), the visible dataset was augmented with CTX image P02_001738_2671 (Malin, 2007; Fig. 2a).

In the inter-trough region adjacent to the imaged and modeled outcrop, more than forty SHARAD observations have been selected for use in subsurface stratigraphic mapping (Fig. 1b). SHARAD operates with a 20-MHz center frequency and a 10-MHz bandwidth, yielding a theoretical vertical resolution of 8.5 m in water ice (Seu et al., 2007). Lateral resolution is 3–6 km in the cross-track direction and 0.3–1 km in the along-track direction (Seu et al., 2007). Observations were chosen based on clarity of the subsurface reflectors and proximity to the visible stratigraphic section (Figs. 3 and 4).

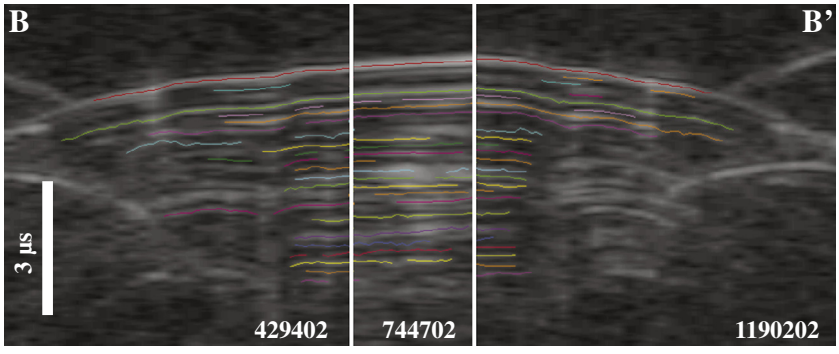

Fig. 4. Three intersecting SHARAD observations of the study site. Vertical white lines denote where the observation changes, representing the intersecting traces or lineties. Colored lines are the semi-automatically picked bright reflectors. The location of transect B to B′ is shown in Fig. 1b.

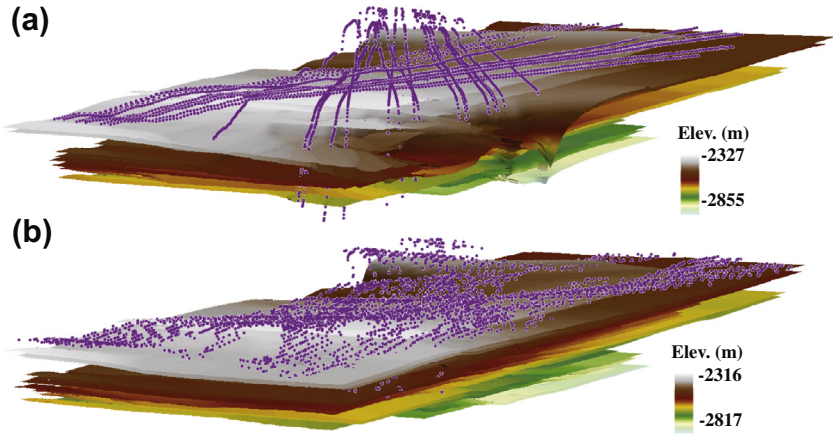

Fig. 5. (a) Subsurface reflectors at the study site modeled with the nadir assumption. Points above the surface are the nadir locations of the first radar returns from the surface. Assuming the first surface echo originates at the nadir point results in artificial surface geometries. (b) Subsurface reflectors modeled using the first surface return algorithm. Taking surface topography into account when calculating the location of the first radar return from the surface results in a more correct subsurface geometry. Location and orientation of reflectors are given in Fig. 7.

4. Radar methods

The stratigraphy revealed by ice-penetrating radar provides a rich history of deposition and erosion (Holt et al., 2010). Often, in order to decipher this history, it is necessary to construct a three-dimensional representation of the subsurface material interfaces that result in reflectors. As a nadir-pointing instrument, one observation by SHARAD records two-dimensional depth-time information with minimal information on lateral variation. In order to convert the two dimensions of individual observations into three dimensional subsurface interfaces, tens to hundreds of intersecting subsurface observations must be utilized.

4.1. Mapping reflectors

Cross-sectional radar images of the subsurface are constructed for each observation by horizontally building up vertical samples, or traces, of time vs. amplitude data and applying a color scale to the amplitude values (Putzig et al., 2009). Visible features are then interpreted using a seismic interpretation platform, here, Schlumberger Corporation's GeoFrame 4.3. Interpretation consists of selecting traces of a bright reflector at intervals along the reflector's discernible length in a single radar image, or radargram; the software then implements an amplitude-fitting algorithm to evaluate the reflector in the intervening traces within a user-defined vertical time window. This process results in a semi-automatically picked line that is fit tightly to the high-amplitude center of the reflector (Fig. 4).

Where SHARAD observations spatially coincide due to orbital geometry, radargrams can be displayed side-by-side at the trace of intersection (Fig. 4). This allows individual reflectors to be confidently identified on multiple observations. Additionally, true reflectors can often be distinguished from subsurface clutter by consulting simulations that predict clutter features (Holt et al., 2008).

4.2. Constructing reflector surfaces

Exporting the time delay of the interpreted reflectors in each trace for all observations removes interpretations from the seismic environment to undergo further analysis. The resulting product is a collection of points, each of which is associated with a reflector name, a trace number, and a time. Assuming a dielectric constant of 3.1 in water ice (Grima et al., 2009), time is converted to depth; additionally, trace number is converted to the nadir latitude and longitude at the surface using spacecraft navigation files. To position the subsurface reflector, the vertical distance between the surface return and subsurface reflector is calculated; this method assumes that all first echoes returned from the surface originate at the nadir point (Fig. 5a).

The assumption of a nadir first echo surface return poses significant problems for modeling reflector surfaces in three-dimensions, a task that requires accurate positions for each surface and subsurface elevation value. In the case of a flat surface, the nadir assumption is accurate, however, in the presence of even slight surface slopes, first echo returns are more likely to originate from off-nadir sites (Fig. 5b). As a result an algorithm designed to predict the originating locations for each first echo returned from the surface based on spacecraft coordinates and topographic data from the Mars Orbiter Laser Altimeter (MOLA) is implemented when calculating reflector location. Although subsurface interfaces may also slope, causing a similar effect of subsurface off-nadir return, subsurface returns are assumed to originate directly below the first surface return. This has not been found to cause significant error in the upper 500 m of the NPLD, the depth to which this study is primarily concerned (see Section 4.3).

Each reflector, represented by a collection of points recording latitude, longitude and elevation, is imported into ESRI's ArcGIS and displayed with a north polar stereographic projection specific to Mars. Slope, aspect and contour maps of elevation are then constructed based on the point data. Additionally, inverse distance weighting interpolation is used to create grids representing each subsurface reflector. The grids are displayed in three dimensions to visualize subsurface topography (Fig. 5). By using multiple, obliquely-intersecting observations spaced closely together and interpolating between the reflectors, the across-track lateral resolution of the SHARAD data is artificially enhanced.

4.3. Vertical uncertainty

While the first-return algorithm is needed to accurately position reflectors in the horizontal direction, a method is required to establish the vertical uncertainty of reflector elevation values. Well-constrained sources of vertical uncertainty include SHARAD's 8.5 m theoretical vertical resolution, or the minimum separation required to distinguish two interfaces in water ice (Seu et al., 2007), and time sampling resolution of 37.5 ns, or ±1.6 m in water ice. Additionally, the registration of surface radar returns with the MOLA Experiment Gridded Data Records (MEGDR) (Smith et al.,

2003) during the first-return correction and reflector gridding process contributes a ±1 m uncertainty (Smith et al., 2001) to elevation values.

Other potential sources of uncertainty, such as systematic processing errors, wave propagation path in the subsurface, and random error, are more difficult to constrain and, therefore, should be identified empirically. One method for doing so employs the orbital crossover analysis (Smith et al., 2001), which assumes that the elevation at any point on the planet's surface should be consistent when surveyed multiple times by an instrument. In the case of the orbital crossover analysis, differences between elevations measured at the same point on the surface are caused by uncertainties in the orbiter position and orientation. Following the same principle, a reflector in the subsurface should be recorded by SHARAD at the same depth even when measured on multiple observations. Because the surface reflector is registered to the MOLA surface, potential differences in reflector elevation due to uncertainties in the spacecraft position and orientation are eliminated, and any remaining difference in reflector elevation is the result of radar wave propagation path or signal processing.

Six subsurface reflectors varying between mean depths of 44 m and 783 m were mapped continuously in the region between the main lobe of Planum Boreum and Gemini Lingula. This area was chosen based on low surface and subsurface slopes (<1°), the absence of stratigraphic disruption due to troughs, and the lateral clarity of reflectors. Nine observation intersections were identified, and the two-way travel time for each of the six subsurface reflectors was obtained at each intersecting trace and the adjacent trace to either side. This resulted in six time delay values for each of the six subsurface reflectors at all nine of the intersections. Each travel time was then normalized to the surface return, and the difference in time delay was taken between corresponding reflectors in corresponding traces from intersecting observations.

The difference, or offset, in mean time delay between reflectors that are expected to be at the same time delay increases from 0 ns at the surface to 22 ns for the deepest reflector studied (Fig. 6a). Increasing reflector offset correlates to increasing depth with an R^2 value of 0.67. It is important to note, however, that all values of mean time delay offset fall below SHARAD's time sampling resolution of 37.5 ns. Therefore, in this case the values obtained for offset do not add additional vertical uncertainty. The increasing offset values do, however, suggest that variation in subsurface pulse propagation path should be taken into account for the deepest reflectors of the NPLD. The linear increase of reflector offset variance with depth supports this conclusion (Fig. 6b). Variance increases with a correlation coefficient of $R^2 = 0.90$ from a value of 0 ns at the surface to 50 ns for the deepest reflector. In this case, the largest standard deviation value, 50 ns, is larger than the time sampling resolution of SHARAD, indicating that time delay measurements for reflectors as deep as 783 m can demonstrate additional vertical uncertainty that is likely caused by variation in pulse propagation path. These results suggest, however, that vertical uncertainty due to pulse propagation path in the upper ~500 m of the NPLD is negligible.

Therefore, theoretical bandwidth-limited resolution, time sampling and MOLA surface registration are the only identified sources of vertical error in the stratigraphic section studied. When added in quadrature, these sources result in a vertical uncertainty of ±4.7 m for SHARAD reflectors analyzed with the methods presented here; note that other methods of interpreting and registering reflectors might lead to minor differences in vertical uncertainty. It is, however, clear that the theoretical resolution (±4.25 m) dominates uncertainty in the near subsurface and provides a good estimation of the uncertainty measurement when other values (e.g. pulse propagation path and radar processing) are not as well constrained.

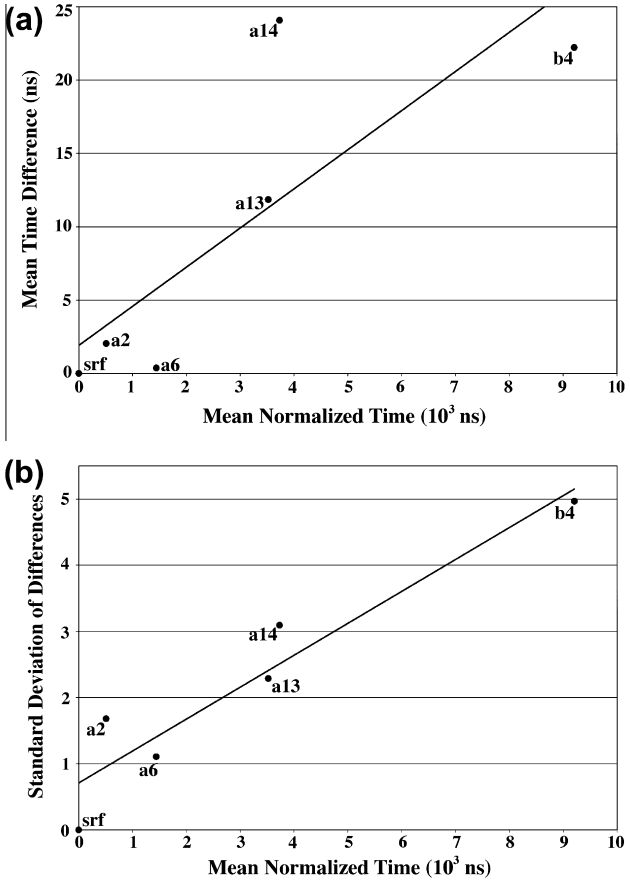

Fig. 6. (a) Mean difference in time delay between the same reflector on multiple SHARAD observations at their point of groundpath intersection plotted against the averaged time delay of the reflector. (b) Standard deviation of time difference plotted against mean time delay of the reflector. Measurements were made in the saddle region between the main lobe of Planum Boreum and Gemini Lingula, where subsurface clutter is minimal and reflectors are continuous for 100s of kilometers.

5. Subsurface analysis and topographic comparison

Based on the results of along-trough elevation profiling of visible layers and planar extrapolations of layers between exposures, the accepted regional model of internal layer structure suggests that layers dip equatorward at less than 1° (Fishbaugh and Hvidberg, 2006). From layer boundary elevations obtained using MOC imagery co-registered with MOLA, variations in layer thickness have been reported, implying local variation in accumulation rates (Fishbaugh and Hvidberg, 2006). Layer pinch-outs and truncation surfaces are also present in the visible stratigraphic record (Tanaka et al., 2005, 2008; Fishbaugh and Hvidberg, 2006). Qualitatively, these characteristics, including low slopes (Smith and Holt, 2010), variation in relative accumulation rates (Putzig et al., 2009), and pinch-outs and truncation surfaces (Holt et al., 2010) have been observed by SHARAD in the subsurface. The observed regional similarities between layers and reflectors warrant a more quantitative comparison between reflector topography and geometry and the same properties for visible layers.

Twenty-five subsurface reflectors were interpreted on 45 SHARAD observations to construct a gridded subsurface volume to a depth of ~600 m over an area of 1450 km^2 (Fig. 5). The average dip of the 25 reflectors is 0.4° to the south. At the regional scale, this result agrees with the <1° slopes of modeled visible layers (Fishbaugh and Hvidberg, 2006). Consistent with the hypothesis of lateral variations in relative accumulation rates, but not explicitly explored for visible layers due to the limitation of

closely-spaced exposures, the gridded reflectors exhibit changes in topography over scales of meters to kilometers. Topographic variation at the 10s of kilometer scale horizontally is consistent between subsurface reflectors (Fig. 7a and b), but local variation in accumulation is suggested by the changing difference between the two reflectors (Fig. 7c). In the case of this particular study site, the zone of increased thickness corresponds with a slope facing away from the equator (reflectors sloping towards A in Fig. 3), which suggests local topography controls accumulation.

While the mean geometries of reflectors and layers agree, it is important to determine if the local subsurface topographic trends revealed by SHARAD are also followed by visible layers. To compare topographic trends between surface and subsurface data, distance–elevation profiles of layers were constructed using CTX image P02_001738_2761 (Fig. 8a); original layers interpreted in the HiRISE DEM (Fishbaugh et al., 2010a) could not be used because the small spatial extent of the DEM did not model a long enough exposure for significant comparison. The CTX image was processed using the Integrated Software for Imagers and Spectrometers version 3 (ISIS 3), an in-house software developed by the U.S. Geological Survey (USGS) for the processing of imagery collected by NASA planetary missions. Image P02_001738_2761 was imported to ISIS 3, radiometrically calibrated, striping was removed, and the image was projected using the north polar stereographic projection for Mars. Following processing, the image was co-registered with MOLA topography in the ArcGIS software. Elevations of CTX layer boundaries were extracted from underlying MOLA topography at 10 km intervals along 75 km of the trough exposure. Distances were measured following the curvature of layers, and thus are not straight-line distances but rather along-trough distance (Fig. 8c). A model radar observation subparallel to the trough exposure was constructed by defining a transect through the highest density of SHARAD first returns along the trough-ward edge of the gridded area. Traces falling within 300 m (a value within the lateral resolution of the radar) of the transect were selected, and the elevations of subsurface reflectors in these traces were recorded. To facilitate comparison of layers and reflectors at different elevations and sampled at different along-track distances we overplot their detrended elevations. In order to detrend the elevations for each layer/reflector, a best-fit plane (constructed in polar stereographic space separately for each feature) was subtracted. This procedure removes the elevation offsets between the layers and any long-baseline tilts thus highlighting the local structure of the NPLD. In contrast to the raw elevation profiles, the detrended layer elevations may cross each other when overplotted as the space between adjacent layers thickens and thins with position. Fig. 8c shows these detrended elevations from the SHARAD and CTX profiles offset by 120 m for clarity.

The profile results demonstrate that there is similarity between the long-wavelength (~50 km) topographic variation detected by SHARAD in the subsurface and the trend followed by visible layers at the surface (Fig. 8). On either side of the prominent slope break at ~6 km in the SHARAD profile, the average slopes of reflectors from A–A′ are 0.006° and −0.01°, respectively. These slopes are similarly small as and agree in sign with average CTX/MOLA-derived slopes of 0.0023° and −0.0031° on either side of the slope break at ~9 km, corresponding to the B–B′ direction. Beyond the second slope break at ~26 km, the visible layers record an average slope of 0.0013° (Fig. 8). The average slope of SHARAD reflectors beyond ~10 km is similar, at 0.0009°. It is likely that the ~3 km offset between the 6 km and 9 km slope breaks in the SHARAD profile and the CTX/MOLA profile, respectively, results from changes that occur in the 10 km gap between the two transects. The offset of slope breaks in addition to meter and kilometer-scale topographic variation in the subsurface (Fig. 7) emphasizes the variability of topography over distances of less than 10 km and calls into question any confidence in elevations derived from planar extrapolation or reflectors over that distance.

Topographic agreement between reflectors and layers at both the 100s of kms and the 10s of kms scales provides strong evidence that reflectors and layers record morphologically related surfaces. Visible layers are currently understood to represent paleosurfaces of the NPLD (Thomas et al., 1992). By structural agreement with visible layering, reflectors can be used as a proxy for visible layer geometry and topography in the subsurface. It is important to note, however, that shared surface morphology does not require reflectors and layers to represent the same surfaces resulting from the same material changes. Therefore, no unique causal relationship is implied by shared morphology.

6. Signal analysis

The effort to find a climate signal in the NPLD has prompted spectral analyses of albedo-depth profiles using MOC images (Laskar et al., 2002; Milkovich and Head, 2005; Perron and Huybers, 2009). Of these studies Fourier analyses conducted on images at the current study site and in adjacent troughs returned prominent

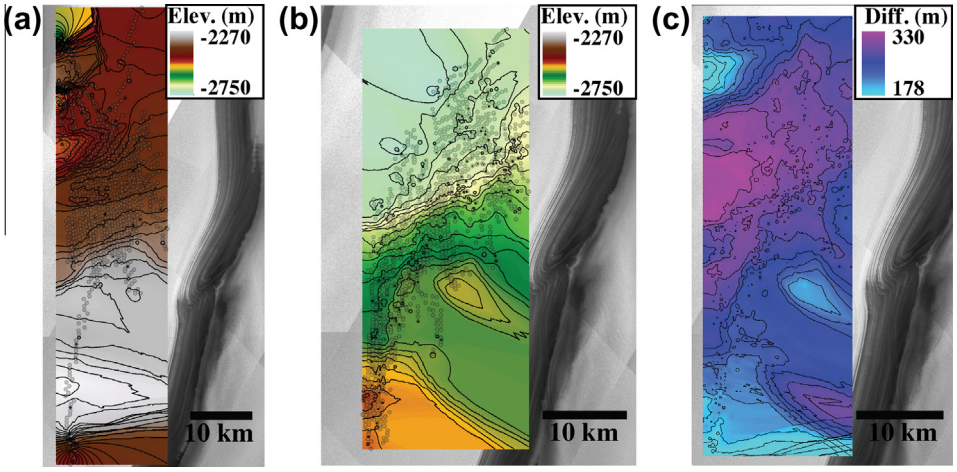

Fig. 7. Gridded subsurface reflectors contoured at 10 m intervals. Reflectors are the (a) first and (b) 20th in the interpreted stratigraphic sequence, and (c) the difference between the two. Note the kilometer-scale topography, as well as the variability in modeled elevation differences. Interpreted radar returns used to grid each reflector are visible as gray points in (a and b). The distribution of points determines how well a subsurface plane extrapolated to the exposure would reflect true subsurface geometry; in these cases, the lack of points near the outcrop prevents a reliable extrapolation.

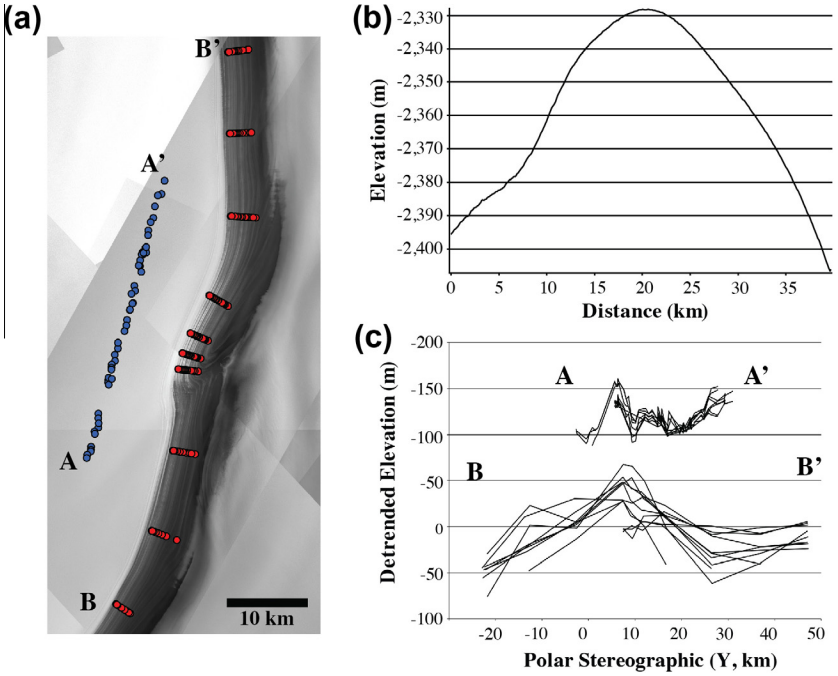

Fig. 8. (a) Locations at which elevation data were taken for the SHARAD subsurface planes (blue points) and visible layers (red points). (b) MOLA surface elevation along the line from A to A′, parallel to the B to B′ transect. (c) Detrended elevations of reflectors (A to A′) and layers (B to B′). SHARAD reflectors are the upper set, and have been offset from the visible layers elevations by 120 m for clarity.

wavelengths of ~33, ~24, and ~21 m in addition to a broad peak between ~15 and 18 m (Milkovich and Head, 2005). If radar and optical layering share a genetic link, similar wavelengths are expected to exist in reflectors at the same site.

6.1. Fourier analysis

The uninterpreted radar trace containing amplitude data vs. time delay is analogous to the albedo-depth profiles extracted from MOC images (Laskar et al., 2002; Milkovich and Head, 2005; Perron and Huybers, 2009), and therefore can be analyzed for comparison with visible wavelengths. A trace ~10 km from the trough exposure was chosen for the frequency analysis based on the clarity and apparent conformity of the subsurface reflectors. All traces within 0.03 km^2, or 0.5% of a Fresnel zone, were aligned with the chosen trace and averaged together in order to create a model radar trace for the current study site (Fig. 1b). Surface effects due to the greater dielectric contrast between ice and free space were minimized by removing data exhibiting high amplitudes related to the first surface return. The resultant model trace was detrended to remove the effects of attenuation with depth, time delay was converted to depth below the surface (assuming water ice), and the 500 m section below the surface was isolated. Because the uncertainties associated with the interpretation algorithm (e.g., surface alignment) do not apply to the construction of the model trace, the average of the resulting wavelengths is reliable down to the vertical resolution limit of SHARAD in water ice, or 8.5 m.

A fast Fourier transform (FFT) for the model radar trace returned peak values at 31, 21, 18 and 16 m, with a broader peak between 24 and 29 m (Fig. 9). These wavelengths correspond most closely to the ~24, ~21 and ~18 m visible wavelengths detected at the adjacent trough (Milkovich and Head, 2005). The similarity between power spectra suggests that the recurrence of visible layers shares similar recurrence values with radar reflectors. These results imply that layers and reflectors share common vertical recurrence distances, providing the first numerical evidence supporting the hypotheses that reflectors and layers are related not only through paleosurface morphology, but also by an underlying formation mechanism that responds to the same environmental forcing.

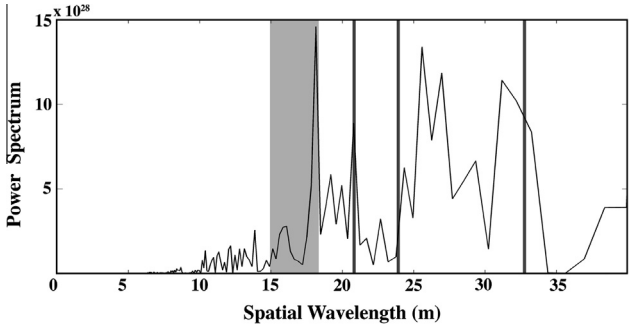

Fig. 9. Spatial wavelengths detected in the upper 500 m of a model SHARAD trace averaged from multiple traces. Location of the model trace is given in Fig. 1b. Vertical gray lines and bars represent the locations of dominant peaks reported in the analysis by Milkovich and Head (2005).

6.2. Statistical analysis

The FFT analyses of uninterpreted optical and radar data demonstrate that similar characteristic signals exist in both data sets, however, the frequency analysis provides little insight into the stratigraphic context of layering. In an effort to contribute geologic meaning to prominent visible layering, the stratigraphic analysis of layering in the DEM included a *k*-means clustering analysis of the vertical separation distance, or the vertical distance between the lower boundary of one layer to the upper boundary of the subjacent layer (Fishbaugh et al., 2009), between marker beds (Fishbaugh et al., 2010b). The clustering analysis consists of an iterative process wherein the user defines a number of clusters, and the statistical software chooses that same number of random values from within the data set to represent initial cluster centers. Each datum

Table 1
Stratigraphic succession of optical and radar separation distances. Comparison begins at the top of the visible and radar stratigraphic sections and records thickness of material between marker beds or reflectors, respectively, down through the column.

Layer separation difference (±1.4 m)[a,b]	Reflector separation difference (±9 m)[b]
24.5	15
36	18.4
26.4	15.8
14.6	15.9
16	23.5
30	26.7
34.2	30.3
40.1	18.6
28	16.6
21.3	16.3
10.6	19.4
17.2	17.7
31.2	

[a] Separation distance values after Fig. S2 in Fishbaugh et al. (2010b).
[b] Error is propagated from uncertainty in the layer and reflector elevations, respectively.

is then assigned to the nearest cluster center, the cluster mean is calculated, and the data are reassigned to the nearest cluster center based on the new means. The process continues until the clusters means are stable and no datum reassignments are made.

For the visible stratigraphy, the *k*-means clustering analysis on the separation distances between visible layers returned clusters of 6.3, 12.5, 21.0 and 30.7 m (Fishbaugh et al., 2009). It has been noted that the 21.0 m and the 30.7 m separation distances closely resemble the dominant 29 m wavelength as well as the secondary 21 m peak apparent in the Fourier analysis at the same site (Milkovich and Head, 2005; Fishbaugh et al., 2009). These results not only suggest that marker bed separation is related to the albedo signal detected throughout the NPLD (Fishbaugh et al., 2010b), but also suggest that the visible layers defined using topographic and morphologic characteristics reliably influence the surface albedo. Furthermore, the agreement between signals in the uninterpreted albedo profiles and the constructed stratigraphic section serves as verification that layers have been meaningfully interpreted.

A similar verification of radar interpretations with respect to a fundamental signal embedded in the amplitude data can be conducted. In the radar data set, the value of greatest similarity to the vertical separation distance of optical layering is the vertical distance between pairs of radar reflectors. By making this comparison to visible separation distances, we are expressly comparing the vertical spacing of radar reflectors to the recurrence of marker beds.

In order to obtain the vertical distances between reflectors, for each trace containing multiple subsurface reflectors, the elevation difference was taken between each reflector and its subjacent reflector. Difference values from all traces containing the reflector pair were then compiled, and a random sample of 1420 values was selected to prevent biasing towards reflector pairs present in more traces, which would weight the cluster results towards those values. The clustering analysis was performed on 34,080 data points, or 1420 values for each of 24 reflector pairs, using SAS's JMP 7.0. Tests were run with three, four, five and six clusters and, considered alongside cumulative plots, which helped to visualize difference values for which there were more data points, and histograms, five clusters were determined to best represent the distribution of values and their frequencies. Furthermore, it is important to note that cluster mean values do not shift significantly when clusters are added; rather, the additional cluster means reflect previously underrepresented concentrations of data.

Note that this method assumes a constant separation distance between reflectors, or else the cluster means would most likely represent the thickening and thinning of material between reflectors. Based on our interpretations, we believe this is a valid assumption for most reflector pairs. In the case of one reflector pair, the upper reflector appears to terminate against the lower reflector, and therefore the values for that pair were omitted from the analysis. Otherwise, the assumption of constant thickness is valid. The clustering analysis on radar reflectors returned values at 11.8, 15.8, 20.3, 27.9, and 35.3 m. These values agree closely with optical data, notably the 21 and 29 m spectral wavelengths and the 12.5 m separation distance.

7. Discussion

Agreement between the qualitative and quantitative characteristics of the radar and visible stratigraphic columns aligns with predictions about the ability to augment surface stratigraphic interpretations with subsurface stratigraphy (Fishbaugh and Hvidberg, 2006). The potential for stratigraphic integration presented here raises new questions concerning the search for a climate signal in the NPLD, the frequency and visible expression of layering, and how far the stratigraphic integration can be taken.

7.1. Climate

In the effort to constrain accumulation rates and NPLD age, the possibility of relating visible layering in the upper kilometer of the deposits to the 51 kyr precession (Laskar et al., 2002), and 120 kyr obliquity (Milkovich and Head, 2005) cycles have been explored. Additional efforts have focused on tying the subsurface packet–inter-packet structure of radar facies to the 2.4 Myr eccentricity modulation period or low-obliquity phases (Phillips et al., 2008), and the relationship of regional patterns in the radar stratigraphy have been compared to multiple proposed correlations to orbital periods (Putzig et al., 2009). The range of orbital cycles still under consideration as candidates for causing layering demonstrates the continuing lack of consensus and understanding of how the NPLD respond to climate change.

The detection of the ~12, 21 and 29 m wavelengths and clusters in the radar stratigraphy verifies that both visible layers and reflectors record a signal of interactions between the surface and atmosphere due to changing atmospheric conditions. While it is beyond the scope of this work to propose layer-reflector correlations to orbital periods utilizing both data sets, the addition of radar to stratigraphic interpretation of the NPLD raises new complications in the search for a fundamental climate signal. The detection of previously-identified visible wavelengths in the upper 500 m of the radar stratigraphy provides a length-scale over which atmospheric change occurred that must be integrated with change occurring at the scale of higher-frequency visible layers as well as at the largest scale of the packet and inter-packet radar structures.

Furthermore, while angular truncation surfaces and disconformities (Tanaka et al., 2008) have been widely recognized in the NPLD, and a sequence stratigraphic interpretation of the deposits had been postulated (Cutts and Lewis, 1982), the lateral persistence of erosional surfaces was not verified until SHARAD revealed the subsurface structure of layering (Holt et al., 2010). At the current study site, a radar discontinuity and an unrelated visible unconformity have been independently identified; it is easy to conclude that similar local discontinuities exist elsewhere in the NPLD. When attempting to decipher the climate record, erosional surfaces at regional and local scales must be taken into account.

The confirmation of existing regional and local hiatal surfaces, including disconformities and angular truncation surfaces, at the vertical scale of SHARAD highlights the dominant assumption

underlying correlations of reflectors and layers to orbital periods, namely, that the radar trace or brightness profile contains a record complete enough to draw a connection. The solution to unraveling the correlation of terrestrial deposits to Milankovich cycles lay largely in the ability to use continuous deep ocean records (Imbrie, 1982). The profusion of visible (Tanaka et al., 2008; Fishbaugh et al., 2010a) and radar (Holt et al., 2010) unconformities challenges the ability to find a meaningful, fundamental climate signal in the reflectors and layers of the NPLD.

7.2. Unique solution

While the results of the signal analyses and geometrical arguments support the idea that radar reflectors and visible layers are genetically related, the question remains as to whether or not an individual reflector can be uniquely correlated to one or more distinct visible layers.

7.2.1. Elevation comparison

The direct correlation of reflectors to visible layers requires that at the topographic surface of the NPLD (here, the trough wall) the linear interpretations representing layers and the planar interpretations representing gridded reflectors spatially coincide so that elevation comparisons can be made along the line of intersection. At 87.1°N, 93.0°E, the current study site, an elevation comparison is not possible due to the ~10 km distance between SHARAD returns and the NPLD exposure. As in previous studies where the reflectors did not intersect the surface, planar extrapolation must be used to close the intervening distance between the two stratigraphies (Milkovich et al., 2009). The results of along-trough profiling (Fig. 8) and reflector gridding (Figs. 5 and 7), however, suggest that extrapolation may not be able to reproduce reflector topography with the accuracy required for a reflector-to-layer correlation.

The reflector and layer elevation profiles reveal long-wavelength topography on the horizontal scale of 50 km (Fig. 8). More importantly, gridding of subsurface interfaces reveals lateral topographic variation at scales similar to and shorter than the extrapolation distance (Fig. 7). Contour maps derived from the gridded reflectors demonstrate that elevation changes of >20 m can occur over horizontal distances of ~5 km (Fig. 7). If the vertical scale of subsurface topography were smaller than SHARAD's vertical uncertainty (±4.7 m), an extrapolation could be performed over the required distance with minimal uncertainty. Because topographic variation exceeds SHARAD uncertainty, however, extrapolating the reflector planes by 10 km could potentially smooth topographic features that would influence the elevation at which the reflectors would outcrop. Furthermore, while the elevation of the gridded surfaces within the aerial extent of the SHARAD data points (Fig. 7) are accurate to the resolution of the radar, the extrapolated grids outside of the data point cloud are effectively unconstrained and do not provide reliable elevations. While a direct comparison of reflector elevations to layer boundary elevations is not discounted as a potential method for stratigraphic integration, it is not considered reliable at this study site.

7.2.2. Separation distance matching

The similar results of the *k*-means clustering analyses on the differences between subjacent radar reflectors and the separation distances between marker beds confirms that the material interfaces causing reflectors occur at intervals comparable to those expressed between prominent visible layers. This result suggests that a comparison could be made between the vertical sequence of visible separation distances and the vertical sequence of radar differences. In other words, counting down from the top in stratigraphic succession, the mean differences between subjacent radar reflectors should be similar to the mean separation distances between marker beds. Results from this analysis demonstrate reasonable, although not complete, agreement (Table 1). Of 13 visible layer separation distances and 12 reflector separation distances, eight intervals agree within the compounded error of the radar and optical methods. Note that this does not inherently imply that matched intervals between the radar and visible stratigraphies occur at the same elevations.

While the radar stratigraphy exhibits a similar underlying signal to the visible stratigraphy, and possibly a similar stratigraphic succession, two scenarios remain as possible explanations for the geometric and statistical similarities between stratigraphic sections. The first is the case of the unique correlation, in which the climatic and atmospheric change that causes visible layers concurrently causes the electric change responsible for radar reflectors (e.g., changing dust concentration). In this scenario a radar reflector and its correlative visible layer will represent the same paleosurface. Alternatively, a layer and a reflector may each represent paleosurfaces of the deposit formed at different times, but modulated by the same orbital period. While the second scenario is somewhat harder to conceptualize and has not been considered in depth, given the strong inclination to attribute reflectors to dust concentration, it remains a possibility that we cannot presently exclude.

7.2.3. Resolution

The disparity in resolution between imagery and radar data creates an additional complication in attempting a reflector-to-layer correlation. Because the resolution of SHARAD dominates the vertical uncertainty, a single reflector represents a ±4.7 m range of elevations; the material change causing the reflector cannot be located within that elevation range. A visible layer, on the other hand, can represent a package of material as thin as <1 m (Fishbaugh et al., 2010b), and the interpreted layer boundary that would be correlated to is accurate to within ±1 m (Fishbaugh et al., 2010b). At the present time, it is impossible to determine if a reflector uniquely correlates to one of two visible layers occurring within that reflector's elevation range. The spatial coincidence of multiple visible layers or layer boundaries with the elevation range of an individual reflector calls into question any attempt to conclude that a single layer morphology represents the change of material responsible for radar reflectors.

8. Conclusions

Agreement between the geometric, topographic, frequency and statistical properties of radar reflectors and visible layers provides the first quantitative evidence for a shared origin at the surface of the north polar deposits of these two types of paleosurface. Radar reflectors can be used as a proxy for visible layering in the NPLD subsurface. Furthermore, the radar reveals the expected, but uncharacterized, presence of local subsurface structure (e.g., disconformities, topographic variation) resulting from spatially-varying accumulation patterns of the NPLD.

Meter- and kilometer-scale relief on subsurface interfaces, as well as stratigraphic features such as disconformities, underscore the importance of using multiple observations when studying the subsurface of even a limited area. The three-dimensionality of the subsurface environment necessitates a high density of data, as well as accurate data positioning through predicting the influence of surface topography on the originating location of the first surface return. Both of these considerations must be made when attempting to accurately interpolate and visually represent subsurface material interfaces.

Extrapolation of gridded subsurface interfaces to the nearest outcrop for correlation to visible layers is similarly complicated.

The orbital geometry of the sounding radar influences the angle at which the outcrop is approached; in many cases, the signal is lost many kilometers from the outcrop due to surface slopes, and the subsurface interface must be extended over distances large enough to include significant relief on the reflector surface, leading to uncertainty in the projected elevation at the outcrop. Therefore, despite the agreement between fundamental characteristics of visible and radar stratigraphies, a unique solution correlating each radar reflector with one or several visible layers remains to be discovered.

Due to the difficulties in conducting a unique correlation at the present study site, including kilometer-scale topography as well as visible angular truncation surfaces and a radar disconformity, analysis at a second study site using the same methods is underway (Russell et al., 2011; Christian et al., 2011). The factors at the current site that inhibit a unique correlation will be largely mitigated at the new site by a favorable geometry of the radar intersection with the outcrop, which will minimize reflector extrapolation distance, a lack of subsurface structure, and continuity of the reflectors with a substantial region of the NPLD, which will lend insight into accumulation patterns and reflector genesis (Christian et al., 2011). Thus, a unique correlation remains possible. If such a correlation is discovered, the ability to tie a visible layer to a subsurface reflector, which can then be mapped throughout the NPLD and to other outcrops, will aid in the construction of a fully three-dimensional stratigraphic model of the layered deposits.

Acknowledgments

We would like to thank Sarah Mattson, Nathaniel Putzig, Patrick Russell, and Sarah Milkovich for their help in developing this project conceptually, critiquing the results, offering suggestions for improvement, and providing additional raw and processed data. Thanks also to Ken Herkenhoff and T. Charles Brothers, who have contributed alternative methods that advanced the study. Reviews by K. Tanaka and an anonymous reviewer provided additional insight into the discussion and helped to improve the work.

References

Blasius, K.R., Cutts, J.A., Howard, A.D., 1982. Topography and stratigraphy of martian polar layered deposits. Icarus 50, 140–160.

Byrne, S., Ivanov, A.B., 2004. Internal structure of the martian south polar layered deposits. J. Geophys. Res. 109 (E11001). http://dx.doi.org/10.1029/2004JE002267.

Christian, S., Holt, J.W., Byrne, S., Putzig, N.E., Russell, P.S., 2011. Impact of nonuniform accumulation on developing an integrated radar-optical stratigraphy of the north polar layered deposits, Mars. In: 5th Mars Polar Sci. Conf. Abstract 6027.

Cutts, J., 1973. Nature and origin of layered deposits of the martian polar regions. J. Geophys. Res. 78, 4231–4249.

Cutts, J.A., Lewis, B.H., 1982. Models of climate cycles recorded in martial polar layered deposits. Icarus 50, 216–244.

Cutts, J., Blasius, K., Briggs, G., Carr, M., Greely, R., Masursky, H., 1976. North polar region of Mars: Imaging results from Viking 2. Science 194, 1329–1337.

Emiliani, C., 1955. Pleistocene temperatures. J. Geol. 63 (6), 538–578.

Fishbaugh, K., Hvidberg, C., 2006. Martian north polar layered deposits stratigraphy: Implications for accumulation rates and flow. J. Geophys. Res. 111, E06012. http://dx.doi.org/10.1029/2005JE002571.

Fishbaugh, K.E., Hvidberg, C.S., Beaty, D., Clifford, S., Fisher, D., Haldemann, A., Head, J.W., Hecht, M., Koutnik, M., Tanaka, K., 2008. Introduction to the 4th Mars Polar Science and Exploration Conference special issue: Five top questions in Mars polar science. Icarus 196, 305–317.

Fishbaugh, K.E. et al., 2009. The stratigraphic record in the martian north polar layered deposits as measured by high resolution stereo topography. Lunar Planet. Sci. 40. Abstract 1998.

Fishbaugh, K.E., Byrne, S., Herkenhoff, K.E., Kirk, R.L., Fortezzo, C., Russell, P.S., McEwen, A., 2010a. Evaluating the meaning of "layer" in the martian north polar layered deposits and the impact on the climate connection. Icarus 205, 269–282.

Fishbaugh, K.E. et al., 2010b. First high-resolution stratigraphic column of the martian north polar layered deposits. Geophys. Res. Lett. 37, L07201. http://dx.doi.org/10.1029/2009GL041642.

Grima, C. et al., 2009. North polar deposits of Mars: Extreme purity of the water ice. Geophys. Res. Lett. 36, L03203. http://dx.doi.org/10.1029/2008GL036326.

Hays, J.D., Saito, T., Opdyke, N.D., Burckle, L.H., 1969. Pliocene–Pleistocene sediments of the equatorial Pacific: Their paleomagnetic, biostratigraphic, and climatic record. Geol. Soc. Am. Bull. 80, 1481–1514.

Hays, J.D., Imbrie, J., Shackleton, N.J., 1976. Variations in the Earth's orbit: Pacemaker of the Ice Ages. Science 194 (4270), 1121–1132.

Herkenhoff, K.E., Murray, B.C., 1990. Color and albedo of the south polar layered deposits on Mars. J. Geophys. Res. 95 (B2), 1343–1358.

Herkenhoff, K.E., Byrne, S., Russell, P.S., Fishbaugh, K.E., McEwen, A.S., 2007. Meter-scale morphology of the north polar region of Mars. Science 317, 1711–1715.

Holt, J.W. et al., 2008. Radar sounding evidence for buried glaciers in the southern mid-latitudes of Mars. Science 322, 1235–1238.

Holt, J.W. et al., 2010. The construction of Chasma Boreale on Mars. Nature 465, 446–449.

Imbrie, J., 1982. Astronomical theory of the Pleistocene Ice Ages: A brief historical review. Icarus 50, 408–422.

Imbrie, J., Imbrie, J.Z., 1980. Modeling the climatic response to orbital variations. Science 207 (4434), 943–953.

Kukla, G.J., 1977. Pleistocene land–sea correlations. I. Europe. Earth-Sci. Rev. 13, 307–374.

Laskar, J., Levrard, B., Mustard, J.F., 2002. Orbital forcing of the martian polar layered deposits. Nature 419, 375–377.

Malin, M., 2007. MRO Context Camera Experiment Data Record Level 0 V1.0. NASA Planetary Data System, MRO-M-CTX-2-EDR-L0-V1.0.

Malin, M.C., Edgett, K.S., 2001. Mars Global Surveyor Mars Orbiter Camera: Interplanetary cruise through primary mission. J. Geophys. Res. 106 (E10), 23429–23570.

Malin, M.C. et al., 2007. Context Camera on board the Mars Reconnaissance Orbiter. J. Geophys. Res. 112, E05S04. http://dx.doi.org/10.1029/2006JE/002808.

McEwen, A.S. et al., 2007. Mars Reconnaissance Orbiter's High Resolution Imaging Science Experiment (HiRISE). J. Geophys. Res. 112, E05S02. http://dx.doi.org/10.1029/2005JE002605.

Milkovich, S.M., Head, J.W., 2005. North polar cap of Mars: Polar layered deposit characterization and identification of a fundamental climate signal. J. Geophys. Res. 110, E01005. http://dx.doi.org/10.1029/2004JE002349.

Milkovich, S.M., Head, J.W., Neukum, G., the HRSC Co-Investigator Team, 2008. Stratigraphic analysis of the northern polar layered deposits of Mars: Implications for recent climate history. Planet. Space Sci. 56, 266–288.

Milkovich, S.M., Plaut, J.J., Safaeinili, A., Picardi, G., Seu, R., Phillips, R.J., 2009. Stratigraphy of Promethei Lingula, south polar layered deposits, Mars, in radar and imaging data sets. J. Geophys. Res. 114, E03002. http://dx.doi.org/10.1029/2008JE003162.

Murray, B.C., Soderblom, L.A., Cutts, J.A., Sharp, R.P., Milton, D.J., Leighton, R.B., 1972. Geological framework of the south polar region, Mars. Icarus 17, 328–345.

Nunes, D.C., Phillips, R.J., 2006. Radar subsurface mapping of the polar layered deposits on Mars. J. Geophys. Res. 111, E06S21. http://dx.doi.org/10.1029/2005JE002609.

Perron, J.T., Huybers, P., 2009. Is there an orbital signal in the polar layered deposits on Mars? Geology 37 (2), 155–158.

Phillips, R.J. et al., 2008. Mars north polar deposits: Stratigraphy, age and geodynamical response. Science 320, 1182–1185.

Picardi, G. et al., 2005. Radar sounding of the subsurface of Mars. Science 310, 1925–1928.

Putzig, N.E., Phillips, R.J., Campbell, B.A., Holt, J.W., Plaut, J.J., Carter, L.M., Egan, A.F., Bernardini, F., Safaeinili, A., Seu, R., 2009. Subsurface structure of Planum Boreum from Mars Reconnaissance Orbiter Shallow Radar soundings. Icarus 204, 443–457.

Russell, P.S. et al., 2011. Mars north polar layered deposit stratigraphy near Gemini Lingula from HiRISE imagery and DTMs. Lunar Planet. Sci. 42. Abstract 2752.

Seu, R. et al., 2007. SHARAD sounding radar on the Mars Reconnaissance Orbiter. J. Geophys. Res. 112, E05S05. http://dx.doi.org/10.1029/2006JE002745.

Shackleton, N., 1967. Oxygen isotope analyses and Pleistocene temperatures re-assesed. Nature 215, 15–17.

Shackleton, N.J., Opdyke, N.D., 1973. Oxygen isotope and paleomagnetic stratigraphy of equatorial Pacific core V28-238: Oxygen isotope temperatures and ice volumes on a 10^5 year and 10^6 year scale. Quatern. Res. 3, 39–55.

Smith, I.B., Holt, J.W., 2010. Onset and migration of spiral troughs on Mars revealed by orbital radar. Nature 465, 450–453.

Smith, D. et al., 2001. Mars Orbiter Laser Altimeter: Experiment summary after the first year of global mapping of Mars. J. Geophys. Res. 106, 23689–23722.

Smith, D., Neumann, G., Arvidson, R.E., Guiness, E.A., Slavney, S., 2003. Mars Global Surveyor Laser Altimeter Mission Experiment Gridded Data Record. NASA Planetary Data System. MGS-M-MOLA-5-MEGDR-L3-V1.0.

Tanaka, K.L., Fortezzo, C.M., 2012. Geologic Map of the North Polar Region of Mars: U.S. Geological Survey Scientific Investigations Map 3177, pamphlet 11 p., 1 sheet, scale 1:2,000,000. <http://pubs.usgs.gov/sim/3177/>.

Tanaka, K., Skinner, J., Hare, T., 2005. Geologic Map of the Northern Plains of Mars. US Geol. Surv. Sci. Invest. Ser. Map SIM-2888.

Tanaka, K., Rodriguez, J.A.P., Skinner, J., Bourke, M., Fortezzo, C., Herkenhoff, K., Kolb, E., Okubo, C., 2008. North polar region of Mars: Advances in stratigraphy, structure, and erosional modification. Icarus 196, 318–358.

Thomas, P., Squyres, S., Herkenhoff, K., Howard, A., Murray, B., 1992. Polar deposits of Mars. In: Kieffer, H., Jakosky, B.M., Snyder, C.W., Matthews, M.S. (Eds.), Mars. Univ. of Arizona Press, Tucson, pp. 767–795.